J of Astronaut Sci (2014) 61:85–106
DOI 10.1007/s40295-015-0058-9

Sun-Direction Estimation Using a Partially Underdetermined Set of Coarse Sun Sensors

Stephen A. O'Keefe[1] · Hanspeter Schaub[2]

Published online: 25 September 2015

Abstract A comparison of different methods to estimate the sun-direction vector using a partially underdetermined set of cosine-type coarse sun sensors (CSS), while simultaneously controlling the attitude towards a power-positive orientation, is presented. CSS are commonly used in performing power-positive sun-pointing and are attractive due to their relative inexpensiveness, small size, and reduced power consumption. For this study only CSS and rate gyro measurements are available, and the sensor configuration does not provide global triple coverage required for a unique sun-direction calculation. The methods investigated include a vector average method, a combination of least squares and minimum norm criteria, and an extended Kalman filter approach. All cases are formulated such that precise ground calibration of the CSS is not required. Despite significant biases in the state dynamics and measurement models, Monte Carlo simulations show that an extended Kalman filter approach, despite the underdetermined sensor coverage, can provide degree-level accuracy of the sun-direction vector both with and without a control algorithm running simultaneously. If no rate gyro measurements are available, and rates are partially estimated from CSS, the EKF performance degrades as expected, but is still able to achieve better than 10° accuracy using only CSS measurements.

✉ Stephen A. O'Keefe
saokeefe@gmail.com

Hanspeter Schaub
hanspeter.schaub@colorado.edu

[1] Aerospace Engineering Sciences, University of Colorado, Boulder, CO, USA

[2] Aerospace Engineering Sciences, American Astronautical Society Fellow, University of Colorado, Boulder, CO, USA

Keywords Coarse sun sensors · Sun-direction estimation · Simultaneous estimation and control

Introduction

In recent years there has been a significant increase in interest in smaller satellites as lower cost alternative to traditional satellites, particularly with the rise of the CubeSat [1]. There has been a lag in the development of attitude control subsystems in comparison to other systems, such as command and data handling and electrical power systems, which have benefited from advances in commercial electronics [2]. Due to stringent mass, size, and often budget constraints, these small satellites typically rely on simple sensor hardware such as coarse sun sensors (CSS) and magnetometers.

Spacecraft commonly use a multitude of low-cost sun sensors to determine a spacecraft's attitude relative to the sun heading. There are two general types of sun sensors used: digital two-axis sensors and coarse analog cosine-type sensors. Digital two-axis sensors combine two or more image sensors and processing electronics into a single package that provides a complete sun vector. These high accuracy sun sensors often combine multiple measurements [3] or use charge-couple-devices (CCDs) [4] to determine the direction of the Sun. The output vector observation of the sun direction and two or more such vector observations are combined to deterministically solve for the estimated spacecraft attitude using a reference sun-direction vector. Many methods exist for solving such a problem including TRIAD [5], Davenport's Q-Method [6], QUEST [7], FOAM [8], and OLAE [9].

Alternatively, cosine-type CSS output a scalar voltage relative to the angle between the input light and the sensor normal and are attractive due to their very low cost, simplicity to manufacture, small size, and minimal power consumption. These sensors are often used in concert with other sensors during deployment to accurately point the spacecraft's solar arrays at the Sun to achieve power positiveness or to perform coarse attitude determination [10, 11]. Solving for a spacecraft's attitude using only CSS is possible, but requires measurements from multiple sensors and additional information, such as a reference time or orbit determination solution, in order to calculate a reference sun-direction vector. When such information is not available, a relative sun-direction vector can be determined instead of a full attitude. In the absence of noise, the sun direction can be determined geometrically at any particular time if the Sun is simultaneously in the field of view of at least three cosine-type sensors; a more reliable estimate is found if continuous 4πsr coverage is achieved by a minimum of four sensors [12].

Because CSS are relatively inexpensive, it is not uncommon for spacecraft to have a multitude of sensors placed around the exterior to achieve the coverage required for determining the sun direction geometrically. The placement of these sensors is generally an iterative process based on experience and prior designs, but can be optimized through various methods [12, 13]. The addition of so many sensors to the

spacecraft is not without its own set of challenges. The fields of view of the CSS can become blocked by other instrumentation, the CSS can interfere with scientific payloads, cabling must be routed for all sensors, and extra sensors require additional testing time and complexity.

An alternative to using a large number of sensors is to use a sun-direction estimation technique that functions well even with a partially underdetermined[1] set of CSS. If the goal of the spacecraft is to point at the Sun to generate power, such an estimation scheme can be used with a control law and the number of sensors needed in regions far from the desired sun direction in the body frame can be reduced.

This paper reviews several sun-direction estimation techniques that rely only on CSS and angular velocity measurements and function using a partially underdetermined CSS configuration. While CSS are flown regularly, there are very few papers detailing the algorithms used to determine the body-relative sun direction. One reason for this is that commonly sufficient CSS are installed such that the sun direction can be uniquely determined at each control time step [12]. Or, more costly 2D sun sensors are employed which can uniquely determine the sun direction with a single measurement. This decouples the sun-direction estimation from the sun-pointing control effort. In contrast, this paper investigates coarse sun-pointing performance when the cosine CSS based sun-direction estimation and sun-pointing control are performed simultaneously. If the spacecraft sun-relative orientation error is large, even a coarse sun-direction estimate will begin rotating the spacecraft closer towards the desired attitude.

Monte Carlo simulations are employed to study the error in the final attitude relative to a power-positive orientation. The CSS configuration is chosen such that in an acceptable power-positive orientation there are at least three or more CSS seeing the Sun. The various techniques are developed for simultaneous control effort, but their performance without control is provided for comparison. The methods examined include a simple vector average approach, a least squares minimum norm solution, and several Extended Kalman Filter (EKF) approaches. In the later approaches it is of interest how sequential partial sun-direction measurements can be blended with a control simultaneously attempting to orient the spacecraft to a power-positive sun orientation, while the earlier approaches determine the sun-direction estimate purely based on current measurements.

First, a description of the sensors and the spacecraft configuration used are presented. The estimation techniques are outlined and numerical simulation results demonstrating the performance of each approach are presented. This research is focused on nominal performance where a rate gyro is available, but additional results, run without rate gyro measurements, are presented as they illustrate robustness considerations.

[1]The sun direction can generally be uniquely determined, in the absence of noise, at a given time if three or more cosine-type CSS measurements are available. For this research, an underdetermined sensor set is one for which there are spacecraft attitudes where the sun-direction cannot be uniquely determined due to an insufficient number of sensors seeing the Sun.

Cosine Sun Sensor Measurement Model

The low-cost cosine-type CSS used in this study are composed of individual photodiodes with glass covers for filtering out undesired wavelengths and optional baffles for restricting the field of view. Assuming Lambert's cosine law, the solar flux F that impacts a CSS due to the direct solar flux of the Sun $F_\odot$ in the vicinity of the Earth is given by [14]

$$F = F_\odot \left(\boldsymbol{n}^T \frac{\boldsymbol{s}}{\|\boldsymbol{s}\|} \right) \tag{1}$$

where $\boldsymbol{n}$ is the surface normal of the CSS and $\boldsymbol{s}$ is the unit direction vector from the spacecraft to the Sun. The solar irradiance due to the Sun does change with time, but the change is small [15] so $F_\odot$ is assumed constant.

Testing of several CSS in a heliostat shows that the scalar output of a CSS due to direct irradiance is generally well approximated by

$$V = C \left(\boldsymbol{n}^T \frac{\boldsymbol{s}}{\|\boldsymbol{s}\|} + \nu_V \right) \tag{2}$$

where the scale factor

$$C = \frac{F_\odot}{F_{\text{cal}}} \tag{3}$$

is determined during ground testing using a calibration flux F_{cal}. This scalar value is then converted to a voltage measurement using the maximum voltage output of the CSS. The value of F_{cal} may be anywhere between 0 % and approximately 70 % of $F_\odot$ due to location, time of day, cloud cover, and atmospheric conditions, and must be calculated using complex models or a pyrheliometer. A sun-direction estimation algorithm that is insensitive to this calibration parameter will enable significantly simpler, and thus cheaper, CSS calibration and testing procedures.

Solar radiation that impacts the Earth is partially absorbed, partially specularly reflected, and partially diffusely reflected. The diffuse reflectivity of the Earth is known as Earth's albedo. Cosine-type CSS are sensitive to any light and on-orbit the most significant light source other than direct sunlight is light diffusely reflected by the Earth. Solar radiation that is absorbed by the Earth and later radiated at infrared wavelengths is easily filtered through mechanical means while the energy due to specular reflectance is generally small and ignored [16].

Consider the situation shown in Fig. 1, where a spacecraft is located at point B with a CSS whose surface normal is given by $\boldsymbol{n}$; dA is a differential area on the surface of the Earth; $\mathbf{n}_A$ is the surface normal of dA; $\mathbf{s}_\oplus$ is the direction vector from the Earth to the Sun; and $\mathbf{r}_{AB}$ is a vector from dA to the spacecraft. The region $\boldsymbol{A}$ is the surface of the Earth that is both illuminated by the Sun and within the field of view of a CSS

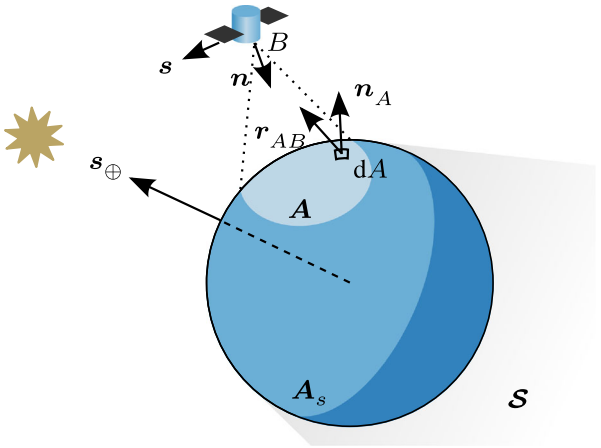

Fig. 1 Illustration of Earth albedo geometry with respect to a satellite in orbit

on the spacecraft. The irradiance received by the CSS due to the diffuse reflectance of the Earth can be calculated as [16, 17]

$$F_\alpha = \frac{F_\odot}{\pi} \int_{\boldsymbol{A}} \frac{\alpha}{\|\boldsymbol{r}_{AB}\|^2} \left(\frac{\boldsymbol{n}_A^T \boldsymbol{s}_\oplus}{\|\boldsymbol{n}_A\| \, \|\boldsymbol{s}_\oplus\|} \right) \left(\frac{\boldsymbol{n}_A^T \boldsymbol{r}_{AB}}{\|\boldsymbol{n}_A\| \|\boldsymbol{r}_{AB}\|} \right) \left(\frac{\boldsymbol{n}^T \boldsymbol{r}_{AB}}{\|\boldsymbol{n}\| \|\boldsymbol{r}_{AB}\|} \right) \mathrm{d}A \quad (4)$$

where α is the albedo, or reflectivity coefficient, of the Earth that varies with $\mathrm{d}A$. It has been shown that the irradiance due to be albedo can be anywhere between 0 % and approximately 50 % of the incident direct solar irradiance with the maximum albedo not at the poles, but over Greenland during local summer at noon [17].

For this work, the value of the Earth's albedo is taken from NASA Total Ozone Mapping Spectrometer mission data. The data used in this study were acquired as part of the NASA's Earth-Sun Division and archived and distributed by the Goddard Earth Sciences (GES) Data and Information Services Center (DISC) Distributed Active Archive Center (DAAC). The value of the Earth's albedo varies significantly with position, and due to seasonal, ground cover, and cloud cover changes so daily measurements from 2000 to 2005, corresponding to a $5^\circ \times 5^\circ$ latitude longitude grid, are used to calculate mean and standard deviation values. These values are used to generate statistically accurate values for the Earth's albedo coefficient used in the numerical simulations.

Taking into account errors in the misalignment of the CSS, the direction vector for a CSS can be spherically expressed as

$$\boldsymbol{n} = \begin{bmatrix} \cos(\phi + \phi_\beta)\cos(\theta + \theta_\beta) & \cos(\phi + \phi_\beta)\sin(\theta + \theta_\beta) & \sin(\phi + \phi_\beta) \end{bmatrix}^T \quad (5)$$

where θ is measured positive from the body $+x$-axis around the $+z$-axis, ϕ is measured positive toward the body $+z$-axis from the $x - y$ plane, and θ_β and ϕ_β are

random constants, with $\mathrm{E}\left[\theta_\beta\right] = 0$, $\mathrm{E}\left[\theta_\beta^2\right] = \sigma_{\beta_\theta}^2$, $\mathrm{E}\left[\phi_\beta\right] = 0$, $\mathrm{E}\left[\phi_\beta^2\right] = \sigma_{\beta_\phi}^2$, $\mathrm{E}\left[\phi_\beta\theta_\beta\right] = 0$, representing misalignment biases.

Adding the CSS misalignment and effects of Earth albedo into Eq. 2, and accounting for the limiting effects of field of view, results in

$$
\begin{aligned}
V &= C \cdot C_\kappa \left(V_d + V_\alpha + \nu_V\right) \\
V_d &= \begin{cases} \boldsymbol{n}^T \frac{\boldsymbol{s}}{\|\boldsymbol{s}\|} & \text{if } \left(\boldsymbol{n}^T \frac{\boldsymbol{s}}{\|\boldsymbol{s}\|} \geq \cos\psi\right) \wedge \left(B \notin \boldsymbol{\mathcal{S}}\right) \\ 0 & \text{if } \left(\boldsymbol{n}^T \frac{\boldsymbol{s}}{\|\boldsymbol{s}\|} < \cos\psi\right) \vee \left(B \in \boldsymbol{\mathcal{S}}\right) \end{cases} \\
V_\alpha &= \begin{cases} -\frac{1}{\pi} \iint\limits_{\boldsymbol{A}} \frac{\alpha}{\|\boldsymbol{r}_{AB}\|^2} \frac{\boldsymbol{n}_A^T \boldsymbol{s}_\oplus}{\|\boldsymbol{n}_A\| \|\boldsymbol{s}_\oplus\|} \frac{\boldsymbol{n}_A^T \boldsymbol{r}_{AB}}{\|\boldsymbol{n}_A\| \|\boldsymbol{r}_{AB}\|} \frac{\boldsymbol{n}^T \boldsymbol{r}_{AB}}{\|\boldsymbol{n}\| \|\boldsymbol{r}_{AB}\|} \mathrm{d}A & \text{if } B \notin \boldsymbol{\mathcal{S}} \\ 0 & \text{if } B \in \boldsymbol{\mathcal{S}} \end{cases}
\end{aligned}
\tag{6}
$$

where ψ is the half angle of the sensor's field of view, and C_κ is a constant random scale factor included to account for error in the knowledge of the calibration coefficient with $\mathrm{E}\left[C_\kappa\right] = 1$ and $\mathrm{E}\left[C_\kappa^2\right] = \sigma_{C_\kappa}^2$. Other hardware limitations, such as obstructions due to solar panels or instrumentation, may also need to be taken into account. For this work it is assumed that the calibration coefficient of all CSS can be defined by the combination of a common, C, and individual, C_κ, component. The common calibration factor is the result of a difference between the flux used to calibrate all the sensors and that experienced on orbit, due to such effects as atmospheric attenuation during calibrations and temporal variations in the solar cycle, whereas the individual factor is due to physical differences between individual sensors. Over time, radiation and other factors may cause the parameters C and C_κ to change, but they are assumed constant over the time scales of interest.

Coarse Sun Sensor Configuration

The spacecraft used for this study is assumed to be equipped with only eight cosine-type CSS in a dual pyramid configuration. Sensors with 120° edge-to-edge fields of view are arranged on the $+z$ and $-z$ faces of the spacecraft oriented 90° apart and angled 45° from the body z axis. An illustration of this configuration is shown in Fig. 2a. Multiple sensor coverage is provided along, $+z$, and opposite, $-z$, the solar array normal direction with minimal coverage along the equator of the spacecraft. This configuration leaves the sides of the spacecraft clear for scientific instrumentation and seeks to minimize both the CSS obstruction due to the solar arrays and the amount of internal cabling necessary for the sensors.

Figure 2b shows the number of CSS to which the Sun is visible for any relation of the Sun with respect to the spacecraft. Note that the fields of view of the CSS are clipped at the local-horizontal plane by the spacecraft structure and solar panel arrays. A Lambert cylindrical area preserving projection [18] is used so as to give a fair relative area comparison of the over, uniquely, and underdetermined regions of

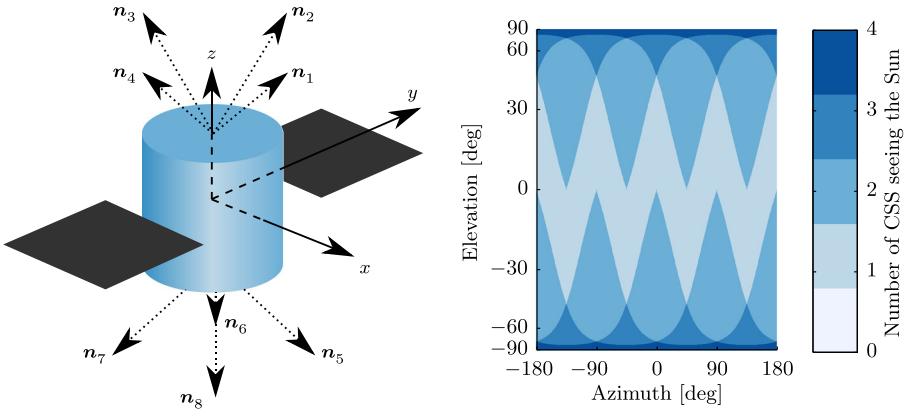

(a) Schematic of spacecraft.

(b) CSS coverage map.

Fig. 2 Illustration of spacecraft, with CSS unit vectors, for an offset dual pyramid configuration and the associated coverage map

coverage. Note that here the ideal sun-pointing direction for a power-positive orientation has an elevation angle of 90°. It is not necessary to have the spacecraft point directly to the sun; being off by 20° to 30° is often acceptable for sufficient power generation.

Sun Direction Estimators

It is important to note that accounting for the effects of Earth albedo in the measurement model of the CSS requires both orbital position information and a inertial reference sun-direction vector. For this work, it is assumed such information is not available; an example of such a situation being immediately after launch vehicle separation before ground communication has been established or an orbit determination solution has been calculated. Thus, for the estimators that follow the input due to Earth's albedo must be treated as a systematic bias V_{α_β} and Eq. 6 is changed to

$$V = C \cdot C_\kappa \left(V_d + V_{\alpha_\beta} + \nu_V\right)$$
$$V_d = \begin{cases} \boldsymbol{n}^T \frac{\boldsymbol{s}}{\|\boldsymbol{s}\|} & \text{if } \left(\boldsymbol{n}^T \frac{\boldsymbol{s}}{\|\boldsymbol{s}\|} \geq \cos\psi\right) \wedge (B \notin \boldsymbol{\mathcal{S}}) \\ 0 & \text{if } \left(\boldsymbol{n}^T \frac{\boldsymbol{s}}{\|\boldsymbol{s}\|} < \cos\psi\right) \vee (B \in \boldsymbol{\mathcal{S}}) \end{cases} . \tag{7}$$

Despite this significant assumption, the estimation algorithms developed here are shown to perform coarse sun-direction estimation adequate for satellite health monitoring and safe-mode maneuvering to power-positive orientations. In addition the quantity

$$\boldsymbol{d} \equiv C\boldsymbol{s} \tag{8}$$

is defined as a scaled sun-direction vector where, as noted earlier, it is assumed that all CSS share a common gross calibration factor C and some individual variation C_κ from this value.

Weighted Average (WAVG) Method

A simple deterministic estimate for the sun-direction vector is formed by taking a vector average of all the CSS capable of seeing the Sun at a single time using

$$\hat{\boldsymbol{s}} = \frac{\sum_{i=1}^{N} \hat{C}_{\kappa_i} V_i \hat{\boldsymbol{n}}_i \, [V_i > 0]}{\left\| \sum_{i=1}^{N} \hat{C}_{\kappa_i} V_i \hat{\boldsymbol{n}}_i \, [V_i > 0] \right\|} \tag{9}$$

where Iverson bracket notation [19] is used, N is the total number of CSS, $\hat{C}_{\kappa_i}$ is the best estimate of the individual calibration scale factor of the ith CSS, and the direction vectors of the CSS seeing the Sun are "weighted" by their measured values. Nominally the bias parameters are set to $\hat{C}_{\kappa_i} = 1.0$, $\hat{\theta}_\beta = 0.0$, and $\hat{\phi}_\beta = 0.0$, but they should be adjusted if better estimates become available. Since the weighted average method is a deterministic approach, the noise-free error of this method is easily calculated for any orientation of the Sun relative to the spacecraft; the resulting error map is shown in Fig. 3.

Figure 3 shows a large band near the equator of the spacecraft in which the error is greater than 30°. If the Sun is within this region, about 90° from the desired orientation, a large estimation error will result. But when coupled with a control algorithm, even an approximate sun-direction estimate provides enough knowledge to apply the appropriate control effort. The desired attitude of the spacecraft requires the sun-direction vector be aligned with the $+z$ axis; shown in Fig. 3, the WAVG method maintains an error of less than 10° when aligned to within 19° of the reference axis. Thus, the estimate becomes more precise near the goal orientation.

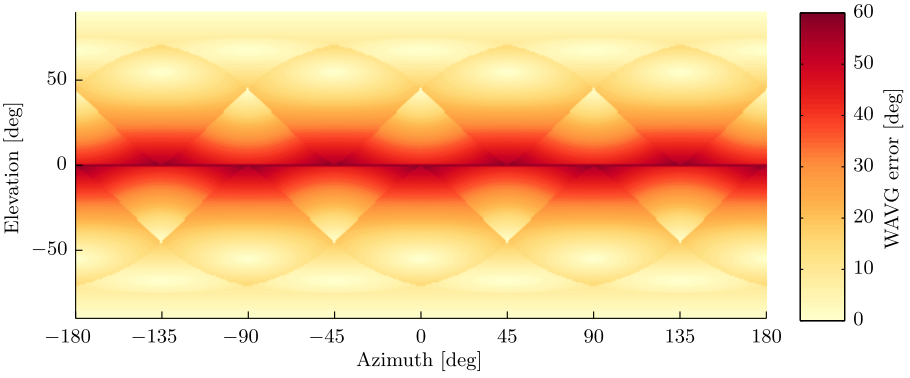

Fig. 3 Weighted average method error map for any relation of the Sun with respect to the spacecraft assuming no noise

This weighted average method is attractive as it is computationally simple, provides an estimate when only one sensor is seeing the Sun, and is ideally capable of estimating the sun-direction vector to within a few degrees using the configuration described previously. Additionally, if the individual CSS calibration factor deviations are assumed small, the gross calibration factor falls out of the formulation, and the WAVG method becomes insensitive to large scale calibration errors common to all sensors.

Least Squares Minimum Norm (LSMN) Method

A more mathematically robust method is the Least Squares Minimum Norm method which combines two methods, least squares and minimum norm, based on the number of CSS measurements available. When the number of measurements available is equal to or greater than three the least squares method is used, and when the system is underdetermined the minimum norm criteria is used.

Starting with Eq. 7, and assuming the input due to albedo[2] V_{α_β} are small, the measurements for the CSS can be written in matrix form as

$$\begin{bmatrix} V_1 \\ \vdots \\ V_N \end{bmatrix} = C \left(\begin{bmatrix} \hat{C}_{\kappa_1} \hat{\boldsymbol{n}}_1^T \\ \vdots \\ \hat{C}_{\kappa_N} \hat{\boldsymbol{n}}_N^T \end{bmatrix} \boldsymbol{s} + \begin{bmatrix} \hat{C}_{\kappa_1} \nu_{V_1} \\ \vdots \\ \hat{C}_{\kappa_N} \nu_{V_N} \end{bmatrix} \right). \tag{10}$$

If the calibration constant C is known, it can be substituted in and these equations solved in a least squares manner for the unit sun-direction vector $\boldsymbol{s}$. However, if C is not known, the equation can be rewritten in terms of $\boldsymbol{d}$ instead

$$\begin{bmatrix} V_1 \\ \vdots \\ V_N \end{bmatrix} = \begin{bmatrix} \hat{C}_{\kappa_1} \hat{\boldsymbol{n}}_1^T \\ \vdots \\ \hat{C}_{\kappa_N} \hat{\boldsymbol{n}}_N^T \end{bmatrix} \boldsymbol{d} + \begin{bmatrix} \nu_1 \\ \vdots \\ \nu_N \end{bmatrix}, \tag{11}$$

giving an implementation that does not require apriori knowledge of the calibration parameter C, again reducing ground calibration requirements. The sun-pointing control, presented later, operates on $\boldsymbol{d}$ as well. If an estimate of C is desired, then it is simply found through $\hat{C} = \|\hat{\boldsymbol{d}}\|$. The measurement equation now is in the traditional least squares form

$$\tilde{\boldsymbol{y}} = H\boldsymbol{x} + \boldsymbol{v} \tag{12}$$

where $\tilde{\boldsymbol{y}}$ is a vector of measured CSS values, H is a mapping matrix, $\boldsymbol{x} = \boldsymbol{d}$ is the state vector, and $\boldsymbol{v}$ is a vector of measurement errors. If there are at least three measurements, the best estimate of the state is given by the least squares solution [20]

$$\hat{\boldsymbol{x}} = \left(H^T H \right)^{-1} H^T \tilde{\boldsymbol{y}}. \tag{13}$$

[2] Assuming the bias due to albedo is small is a significant assumption, however, this leads to a linear form and numerical Monte Carlo results show that the resulting coarse pointing performance, when coupled with a control algorithm, is sufficiently good for coarse sun pointing.

If, however, there are only one or two observations the system is underdetermined and the minimum norm criterion [20]

$$\hat{\boldsymbol{x}} = H^T \left(H H^T \right)^{-1} \tilde{\boldsymbol{y}} \tag{14}$$

is used to determine a unique solution.

The error of the LSMN method is calculated for any orientation of the Sun relative to the spacecraft, in the absence of noise, and is shown in Fig. 4. Comparing Figs. 3 and 4, it can be seen that the LSMN estimate has an error that is equal to or less than the weighted average method for all orientations, and particularly less error, up to 18° less, in regions of only two or three sensor coverage. The large error regions are again near 90° from the desired orientation.

This method is also insensitive to large scale calibration errors, which can reduce costly pre-flight calibration requirements. As long as all CSS are calibrated to return the same value for a given amount of irradiance, and the common calibration factor is set so that the output doesn't saturate, there is no need to know the exact value when pointing straight at the Sun while in orbit. It is important to remember that several key assumptions have been made, most notably negligible calibration errors and biases, that are not always true in flight. However, numerical simulation results, shown later, demonstrate that this method is capable of achieving coarse sun pointing despite these biases.

Weighted Least Squares Minimum Norm (WLSMN) Method

The Least Squares Minimum Norm method is found through numerical simulation to be significantly affected by the systematic biases in the system; in particular it exhibits poor performance when the ratio between the value due to direct sunlight and the value due to Earth's albedo is large. The errors introduced by the inability

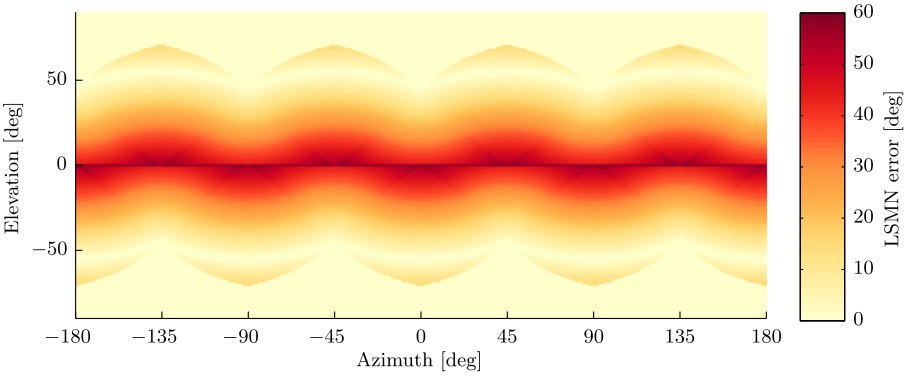

Fig. 4 Least Squares Minimum Norm method error map for any relation of the Sun with respect to the spacecraft assuming no noise

to properly model the affect of Earth albedo, due to a lack of information, can be somewhat mitigated by using a weighted least squares solution [20]

$$\hat{\boldsymbol{x}} = \left(H^T W H\right)^{-1} H^T W \tilde{\boldsymbol{y}} \tag{15}$$

where W is a diagonal weighting matrix usually chosen as the inverse of the noise variance. Because this only applies when noise is present, it does not change the error map shown in Fig. 4, and this modification retains the desirable property of being robust to gross calibration errors common to all CSS.

As a result of the case statements in the measurement model, any measurements coming from sensors not pointed at the Sun are assumed noise. In addition, because the CSS are assumed to provide only positive measurements, these noisy measurements will always be biased. Therefore, to reduce the impact of these highly uncertain measurements on the estimate, the weights of the individual CSS are set to their measured value. Using this approach the stronger signals from sensors seeing the sun are weighted more than the weaker unmodeled signals induced by Earth's albedo. This weighting scheme is used here as illustrative, and should be adjusted based on the goals of a mission. For example, setting the weights to the square or cube of the measured value improves steady state performance when coupled with simultaneous control and a fully determined goal orientation, but degrades the performance when uncontrolled.

Extended Kalman Filter (EKF) Method

A common attitude estimation problem involves propagating the state dynamics and correcting that estimate using a direct measurement of the body's attitude. Thus, instead of solving the geometry of the CSS measurement values at any instant in time, sensor measurements are used to correct a propagated estimate of the sun-direction vector. While a single CSS measurement cannot fully determine the sun direction for the partially under-determined CSS configuration used in this study, a series of measurements coupled with the differential rotation information from the rate gyro, can determine the proper sun direction. The following section describes the application of a continuous-discrete extended Kalman filter formulated with non-additive noise to the problem of estimating the scaled sun-direction unit vector in the spacecraft body frame. The reader is referred to References [20], [21], and [22] for more information on the EKF equations and their derivation.

When using a sequential filter to perform attitude estimation it is common to estimate an absolute attitude, expressed as a quaternion or Modified Rodrigues Parameter (MRP) set [23]. It has been shown that one can estimate such an attitude, in addition to scale factor and alignment calibration factors, for CSS [24]. However, this approach requires additional information, such as measurements from a star tracker or orbit information, to generate a reference sun-direction vector. Here the estimation of the sun-direction vector is performed using only measurements from CSS and a rate gyro.

The measurement model in Eq. 7 is used and the state vector is chosen to be the scaled sun-direction vector, defined in Eq. 8, in the body frame

$$\boldsymbol{x}(t) = \left[{}^{\mathcal{B}}\boldsymbol{d}(t) \right] \tag{16}$$

While it may be more optimal to enforce the unit-norm constraint on the unit sun-direction and estimate the common calibration coefficient separately, for a system with only CSS and rate gyro measurements the common calibration coefficient is unobservable. Combining the common scale factor and the unit sun-direction vector into a single vector value results in a quantity that can be estimated, with the added benefit that the estimator is insensitive to uncertainty in the common CSS scale factor.

It is assumed that angular velocity measurements are provided via a rate gyro and that the rate gyro measurements follow Farrenkopf's approximation [25]

$$ {}^{\mathcal{G}}\tilde{\boldsymbol{\omega}}(t) = [GB]\, {}^{\mathcal{B}}\boldsymbol{\omega}(t) + {}^{\mathcal{G}}\boldsymbol{\eta}_{\omega}(t) \tag{17a}$$

$$ {}^{\mathcal{G}}\dot{\boldsymbol{\omega}}_b(t) = {}^{\mathcal{G}}\boldsymbol{\eta}_{\omega_b}(t) \tag{17b}$$

where ${}^{\mathcal{B}}\boldsymbol{\omega}$ is the true body angular velocity in the body frame, ${}^{\mathcal{G}}\tilde{\boldsymbol{\omega}}$ is the measured body angular velocity in the frame of the rate gyro, $[GB]$ maps vectors written in the body frame $\mathcal{B}$ into vectors written in the gyroscope frame $\mathcal{G}$, ${}^{\mathcal{G}}\boldsymbol{\omega}_b$ is the measurement bias, and ${}^{\mathcal{G}}\boldsymbol{\eta}_{\omega}$ and ${}^{\mathcal{G}}\boldsymbol{\eta}_{\omega_b}$ are zero-mean Gaussian white-noise processes with spectral densities given by $\sigma_{\omega}^2 \boldsymbol{I}_{3\times 3}$ and $\sigma_{\omega_b}^2 \boldsymbol{I}_{3\times 3}$, respectively.

Using this rate gyro model, and assuming for time scales of interest the inertial sun vector is constant[3], the dynamics of the scaled sun-direction vector can be written as

$$\frac{{}^{\mathcal{B}}\mathrm{d}}{\mathrm{d}t}\left[{}^{\mathcal{B}}\boldsymbol{d}(t) \right] = {}^{\mathcal{B}}\boldsymbol{d}(t) \times [BG]\left({}^{\mathcal{G}}\tilde{\boldsymbol{\omega}}(t) - {}^{\mathcal{G}}\boldsymbol{\omega}_b(t) - {}^{\mathcal{G}}\boldsymbol{\eta}_{\omega}(t) \right) - {}^{\mathcal{B}}\boldsymbol{\eta}_s(t) \tag{18}$$

where $\boldsymbol{\eta}_s$ is a zero-mean Gaussian white-noise process with $\mathrm{E}\left[\boldsymbol{\eta}_s(t)\, \boldsymbol{\eta}_s(\tau)^T\right] = \sigma_s^2 \delta(t-\tau)\, \boldsymbol{I}_{3\times 3}$. Given the state propagation and update equations

$$\dot{\boldsymbol{x}}(t) = \boldsymbol{f}(\boldsymbol{x}(t), \boldsymbol{u}(t), \boldsymbol{\eta}(t), t), \quad \boldsymbol{\eta}(t) = \left[{}^{\mathcal{B}}\boldsymbol{\eta}_s^T(t)\ {}^{\mathcal{G}}\boldsymbol{\eta}_{\omega}^T(t) \right]^T \tag{19}$$

$$\boldsymbol{y}_k = \boldsymbol{h}_k(\boldsymbol{x}_k, \boldsymbol{v}_k, t_k), \quad \boldsymbol{v}_k = \left[\boldsymbol{v}_{V,k} \right] \tag{20}$$

the key values for the implementation of this EKF include

$$F(t) \equiv \left.\frac{\partial \boldsymbol{f}}{\partial \boldsymbol{x}}\right|_{\hat{\boldsymbol{x}},\boldsymbol{u}} = \left[-\left[[BG]\, {}^{\mathcal{G}}\tilde{\boldsymbol{\omega}}(t) \right]_{\times} \right], \quad \mathrm{G}(t) \equiv \left.\frac{\partial \boldsymbol{f}}{\partial \boldsymbol{\eta}}\right|_{\hat{\boldsymbol{x}},\boldsymbol{u}} = \left[-\boldsymbol{I}_{3\times 3} - \left[{}^{\mathcal{B}}\hat{\boldsymbol{d}}(t) \right]_{\times} [BG] \right] \tag{21a}$$

$$H_k \equiv \left.\frac{\partial \boldsymbol{h}_k}{\partial \boldsymbol{x}_k}\right|_{\hat{\boldsymbol{x}}_k^-} = \left[H_{1,k}^T \cdots H_{N,k}^T \right]^T, \quad M_k \equiv \left.\frac{\partial \boldsymbol{h}_k}{\partial \boldsymbol{v}_k}\right|_{\hat{\boldsymbol{x}}_k^-} = \left\| \hat{\boldsymbol{d}}_k \right\| \boldsymbol{I}_{N\times N}$$

[3] Analysis of ephemeris data shows the actual rate of change of the elements of the inertial sun-direction vector for a spacecraft in a 400km low Earth polar orbit has a maximum absolute value on the order of $1x10^{-7}$.

$$H_{i,k} = \begin{cases} \left[\cos\phi_i \cos\theta_i \;\; \cos\phi_i \sin\theta_i \;\; \sin\phi_i\right] & \text{if } \boldsymbol{n}_i^T \frac{\hat{\boldsymbol{d}}_k}{\left\|\hat{\boldsymbol{d}}_k\right\|} \geq \cos\psi_i \\ \left[0\ 0\ 0\right] & \text{if } \boldsymbol{n}_i^T \frac{\hat{\boldsymbol{d}}_k}{\left\|\hat{\boldsymbol{d}}_k\right\|} < \cos\psi_i \end{cases} \tag{21b}$$

where $[\cdot]_\times$ represents the skew-symmetric cross product matrix given by

$$\boldsymbol{a} = \begin{bmatrix} a_1 \\ a_2 \\ a_3 \end{bmatrix}, \quad [\boldsymbol{a}]_\times = \begin{bmatrix} 0 & -a_3 & a_2 \\ a_3 & 0 & -a_1 \\ -a_2 & a_1 & 0 \end{bmatrix}.$$

For this study, the EKF algorithm is not initialized until at least one sensor registers direct sunlight from the Sun, determined using a simple threshold, and the initial state estimate is calculated using the WLSMN method when this occurs. No a priori knowledge about the common scale factor C is assumed. It should be noted that while this measurement model approximates the physical response of the CSS, if the current estimate of the sun direction is not within the field of view of the sensor the corresponding row of the Kalman gain is equal to zero and the measurement does not impact the current state estimate. This results in strong measurements due to direct sunlight being ignored if the current estimate of the sun direction is in significant error. Therefore, the measurement update is modified to include observations that are above 50 % of the expected maximum output. This improves the performance when initially lost in space and does not impact steady state performance.

Because of the case statements in the CSS measurement equation, uncertainties in misalignment within the expected 1σ limits can lead to errors exceeding the estimated uncertainty. These inconsistent measurements can lead to filter divergence if not taken into account. The maximum angle from the field of view boundary at which inconsistent errors occur γ is modeled by adding the offset angle a 1σ misalignment can impose

$$\gamma_m = \arccos\left(\boldsymbol{n}^T\hat{\boldsymbol{n}}\right) = \arccos\left(\cos\left(\sigma_{\theta_\beta}\right)\cos(\phi)\cos\left(\phi+\sigma_{\phi_\beta}\right) + \sin(\phi)\sin\left(\phi+\sigma_{\phi_\beta}\right)\right) \tag{22}$$

to the angular uncertainty of the current scaled sun-direction estimate. The variance of the angular offset of the sun-direction estimate from a reference unit-vector in the body frame $\boldsymbol{c}$ is given to first order by

$$\boldsymbol{\Sigma}\left(\gamma_{\hat{d}}\right) = J_\gamma P J_\gamma^T$$

$$J_\gamma = \left[\frac{1}{\sqrt{1-\left(\boldsymbol{c}^T\frac{\hat{\boldsymbol{d}}}{\left\|\hat{\boldsymbol{d}}\right\|}\right)^2}}\left(\frac{\hat{\boldsymbol{d}}^T}{\left\|\hat{\boldsymbol{d}}\right\|}\left(\boldsymbol{c}^T\frac{\hat{\boldsymbol{d}}}{\left\|\hat{\boldsymbol{d}}\right\|}\right) - \boldsymbol{c}^T\right)\right] \tag{23}$$

where P is the state covariance matrix. The maximum measurement error is calculated using

$$\max\left(\boldsymbol{y}_k - \hat{\boldsymbol{y}}_k\right) = \sigma_C\sigma_{C_\kappa}\left\{\cos(\psi - \min(\psi,\gamma)) + \sigma_{V_\alpha} + \sigma_{v_V}\right\} \tag{24}$$

In practice, the implementation of increased innovation variance is done through logic statements and a bound larger than 1σ, such as 3σ, must be used to ensure measurement inconsistencies do not drive the filter to divergence.

The rate gyro bias does not represent random Gaussian noise term and is not being estimated. For the configuration considered, both controlled and uncontrolled, the posterior Cramér-Rao lower bound [26–28] calculated using the true trajectory shows using only CSS measurements provides no improvement in the knowledge of the rate gyro bias beyond the initial a priori bound. Similarly, the calibration coefficients β_{C_i}, β_{θ_i}, and β_{ϕ_i}, also represent systematic biases. One common method, and the method used here, of dealing with such biases is suitably inflating the state and measurement process noise through numerical Monte Carlo simulation to ensure the covariance of the system encompasses the expected statistical error due to this bias. It is acknowledged that this method is not optimal, due to the significant nature of the biases, but it does provide a bounded estimate for this system when no other information is available. Alternatively, the statistics of the biases can be used in a consider Kalman filter, that estimates the contribution to the state uncertainty from the bias, but not the bias directly [20, 29, 30].

Numerical Simulation

A spacecraft is modeled in a 400 km altitude circular orbit with an inclination of 90° starting on 2015 June 1, 00:00 UTC. The accelerations due to the J_2 through J_6 Earth zonal gravitational perturbations, atmospheric drag, and solar radiation pressure (SRP) are modeled. The spacecraft is assumed to have a mass of 100 kg, a drag area of approximately 0.38 m^2, a ballistic coefficient of 2.1, and a cross sectional area of 1.3 m^2 subject to SRP. This orbit has a period of approximately 92.5 min and the spacecraft spends approximately 56.6 min in view of the Sun per orbit. The relative positions of the Earth and Sun are simulated using ephemeris from the NASA Navigation and Ancillary Information Facility (NAIF) SPICE toolkit [31].

The spacecraft's initial true anomaly and attitude are uniformly distributed amongst all possible values and its initial angular velocity is uniformly distributed about all three axes with a maximum value of 2.0° /s about each axis. Rate gyroscope measurements are simulated at 10 Hz and the rate white noise standard deviation is assumed to be $1 \times 10^{-4\circ}/\sqrt{s}$ with a drift stability standard deviation of $1 \times 10^{-6\circ}/s$ over 1000 s. The spacecraft inertia is assumed $[I] = \text{diag}\left[\begin{array}{ccc} 10.5 & 8.0 & 7.5 \end{array}\right]$ kg m^2, and the spacecraft is assumed equipped with four reaction wheels for control purposes. In the spacecraft body frame the spin, or alignment, axes $\boldsymbol{g}_s$ for these reaction wheels are given by

$$G_s = \left[\begin{array}{cccc} \boldsymbol{g}_{s_1} & \cdots & \boldsymbol{g}_{s_4} \end{array}\right] = \left[\begin{array}{cccc} 0 & 0 & \cos(45^\circ) & -\cos(45^\circ) \\ \cos(45^\circ) & \sin(45^\circ) & -\sin(45^\circ) & -\sin(45^\circ) \\ \sin(45^\circ) & -\cos(45^\circ) & 0 & 0 \end{array}\right]$$

Each reaction wheel is assumed to have a spin-axis inertia of $J_s = 0.001$ kgm^2 and a maximum torque of 30 mN m.

The alignment azimuth and elevation of each CSS is perturbed by a normally distributed angle with a standard deviation of 1°. All CSS are assumed to be affected by a common uniformly distributed calibration error between 0 % to 50 %, and normally

distributed individual calibration errors with standard deviation of 2.0 %. CSS measurements are processed at 2 Hz and white Gaussian noise is added to each sensor with a standard deviation of 0.05.

Sun-Direction Estimation Without Attitude Control

An initially uncontrolled tumbling spacecraft is simulated to investigate the baseline performance of the various sun-direction estimation methods described if they are not assisted with a simultaneously active attitude control. The resulting statistics for a 1000 case, 100 min, Monte Carlo analysis are shown in Fig. 5. The statistics are calculated for the time the spacecraft has at least one valid CSS measurement; the time spent in the shadow of the Earth has been removed. The results are color coded by estimation method with the mean of the Monte Carlo results shown as a solid line and the 3σ, or 99th percentile, values shown as dashed lines. The average number of CSS receiving direct sunlight throughout the simulation is shown in Fig 5e as reference; because the control is not active the value is the same for all four estimators and remains below two for all time.

While the estimators output a solution for the scaled sun-direction vector, what is of interest is the total angular error of the estimate, calculated as the angle between the estimated sun-direction and the true sun-direction, shown in Fig. 5d. As can be seen, the single-point estimation algorithms, WAVG, LSMN, and WLSMN, all show significant error in the resulting scaled sun-direction vector estimation; the 99th percentile bounds for the estimated angular errors for all three methods are above 45°, and the mean error is approximately 20°. This is expected due to the underdetermined nature of the CSS configuration; the average number of CSS receiving direct sunlight is approximately 1.8 for all cases. This is also evident in the non-zero mean of the sun-direction angular error. The EKF method performs the best, reducing the 99th percentile attitude estimation error to 1.75° within a few minutes, and maintaining that level of accuracy throughout the trajectory.

Closed-Loop Sun-Direction Estimation with Rate Gyro Measurements

A nonlinear three-axis attitude control is used in the numerical simulation to reorient the spacecraft using redundant reaction wheels [32]. This control law is designed for detumbling and its goal is to orient the spacecraft body frame $\mathcal{B}$ with a reference frame $\mathcal{R}$ where the attitude error between the body and reference frames is described using the Modified Rodrigues Parameter (MRP) set $\boldsymbol{\sigma}_{\mathcal{BR}}$. The control law is given by

$$\begin{aligned} G_s \boldsymbol{u}_s = & -[I]\left(\dot{\boldsymbol{\omega}}_r - [\boldsymbol{\omega}]_\times \boldsymbol{\omega}_r\right) + K\boldsymbol{\sigma}_{\mathcal{BR}} + P\Delta\boldsymbol{\omega} + PK_I\boldsymbol{z} \\ & -\left([\boldsymbol{\omega}_r]_\times - [K_I\boldsymbol{z}]_\times\right)\left([I]\boldsymbol{\omega} + G_s\left\{\boldsymbol{J}_s \circ \left(\boldsymbol{\Omega} + G_s^T\boldsymbol{\omega}\right)\right\}\right) + \boldsymbol{L} \end{aligned} \quad (25)$$

where $\Delta\boldsymbol{\omega} = \boldsymbol{\omega} - \boldsymbol{\omega}_r$, $\boldsymbol{\omega}_r$ is a time-varying reference angular velocity, K is a scalar gain, P is a positive definite gain matrix, K_I is a gain matrix, $\boldsymbol{z}$ is the integral term, $\boldsymbol{J}_s$ is a vector of wheel spin-axis inertias, $\circ$ is the Hadamard, or Schur, product [33],

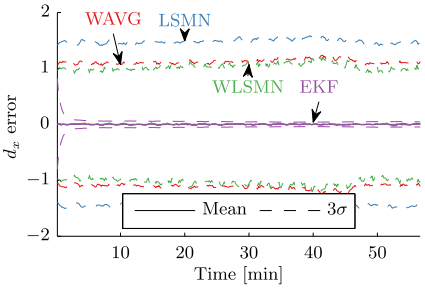

(a) Error in x-component of scaled sun-direction vector.

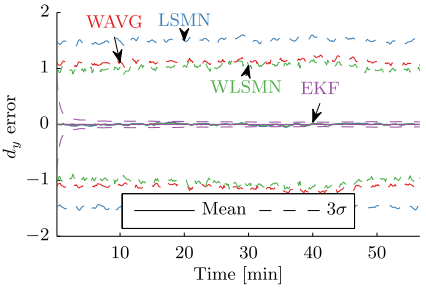

(b) Error in y-component of scaled sun-direction vector.

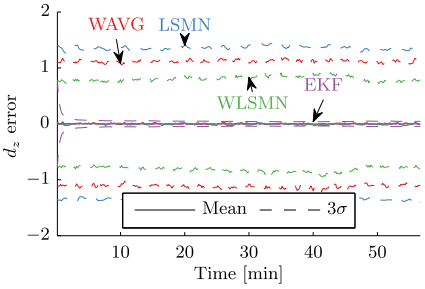

(c) Error in z-component of scaled sun-direction vector.

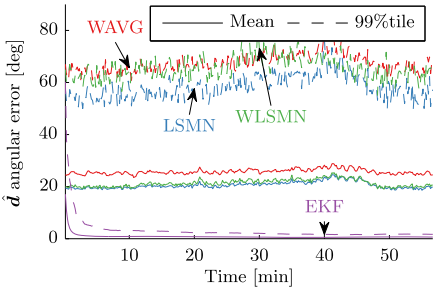

(d) Angular error of sun-direction vector estimate.

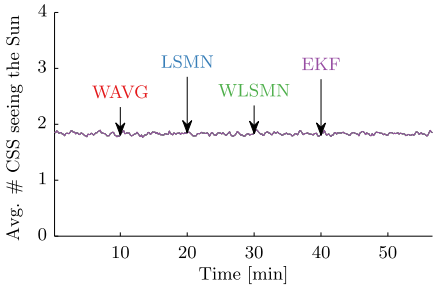

(e) Average number of CSS receiving direct sunlight.

Fig. 5 Calculated statistics for 1000 case Monte Carlo run without control using a dual pyramid CSS configuration

$\boldsymbol{\Omega}$ is a vector of wheel speeds, and $\boldsymbol{L}$ are the known external torques acting on the vehicle. The control is proven to be asymptotically stabilizing and guarantees if $\boldsymbol{\sigma}$ converges to zero, so will $\Delta\boldsymbol{\omega}$. For further discussion of this control law, and its development, the reader is referred to Reference [32]. For this analysis the control gains $K = 0.041\,\mathrm{N\,m}$, $P = 0.5 I_{3\times3}\mathrm{N\,m\,s}$, and $K_I = 0.001 I_{3\times3}/\mathrm{N/s^2}$ are used, $\boldsymbol{\omega}_r = \dot{\boldsymbol{\omega}}_r = \begin{bmatrix} 0 & 0 & 0 \end{bmatrix}^T$, and a control deadband of 1° is used.

The estimation algorithms compute a value for the sun-direction vector in the body frame, not an attitude error. The error MRP $\boldsymbol{\sigma}_{\mathcal{BR}}$ is formed by finding the principal rotation vector necessary to rotate the sun-direction vector to align with the solar

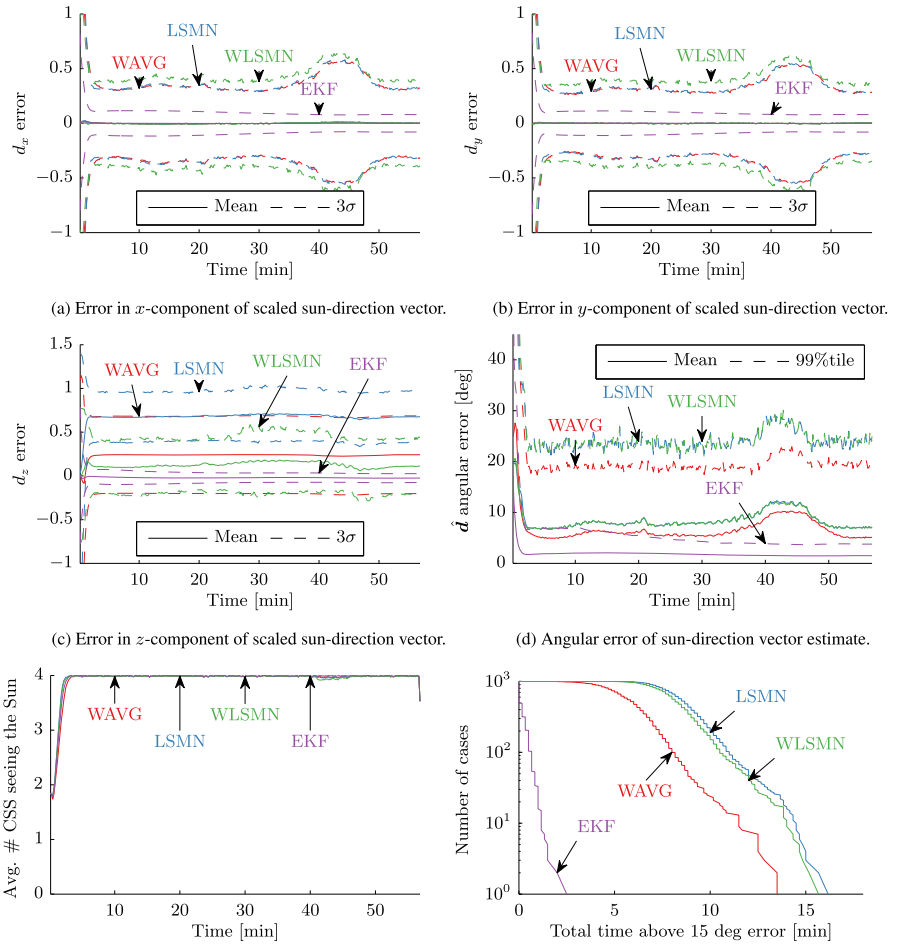

(a) Error in x-component of scaled sun-direction vector.

(b) Error in y-component of scaled sun-direction vector.

(c) Error in z-component of scaled sun-direction vector.

(d) Angular error of sun-direction vector estimate.

(e) Average number of CSS receiving direct sunlight.

(f) Total time spent with estimate in error of greater than 15°.

Fig. 6 Calculated statistics for 1000 case Monte Carlo run with control using a dual pyramid CSS configuration

panel unit normal vector $\boldsymbol{c}$ expressed in the body frame. This vector is then used in the definition of the MRP vector

$$\boldsymbol{\sigma} = \hat{\boldsymbol{e}} \tan\left(\frac{\Phi}{4}\right) \tag{26}$$

to create an error MRP given by

$$\boldsymbol{\sigma}_{\mathcal{BR}} = \frac{\hat{\boldsymbol{d}} \times \boldsymbol{c}}{\left\|\hat{\boldsymbol{d}} \times \boldsymbol{c}\right\|} \tan\left(\frac{1}{4}\cos^{-1}\left(\frac{\boldsymbol{c}^T \hat{\boldsymbol{d}}}{\|\boldsymbol{c}\|\,\|\hat{\boldsymbol{d}}\|}\right)\right). \tag{27}$$

Because of the normalization included in the error MRP this control approach is able to operate on the current scaled sun-direction estimate $\hat{\boldsymbol{d}}$, not the unit

sun-direction vector $\boldsymbol{s}$. Equation 27 can result in a singularity when the denominator approaches zero, or the solar array normal approaches alignment with the sun-direction vector. However, at the same time the trigonometric function in the numerator will also approach zero. This issue is avoided by simply setting the control to zero when the dot product inside the inverse cosine function falls below a threshold.

Figure 6 shows the statistics for a 1000 case Monte Carlo analysis with the nonlinear control turned on; these results emphasize the positive impact of simultaneously estimating and controlling in this partially underdetermined CSS configuration. As noted earlier, the control attempts to orient the spacecraft's solar arrays to be pointed at the Sun while simultaneously estimating the sun direction. Due to the configuration of CSS used, this increases the information content available to the estimator, which is reflected in the increase in CSS seeing the Sun, and the significant decrease in estimation error as compared to the uncontrolled cases. Figure 6f shows the sorted total time above 15° for all the Monte Carlo runs on a log scale where the 15° threshold is an arbitrary limit used for comparison purposes. The discretized nature of the lines in Fig. 6f are a result of the frequency of data output from the simulation. The slight differences between the methods in the average number of CSS receiving direct sunlight is due to the simultaneous control and estimation; the estimators exhibit different initial transient behavior, but all arrive at a steady state solution with an average of four sensors receiving direct sunlight.

All of the estimators are found to spend less than 17 min, of the approximately 56.5 min in view of the Sun for a single orbit, with angular accuracy greater than 15°. The EKF method spends the least amount of time above the threshold, 2 min, and achieves much higher estimate accuracy than the single-point estimators. Interestingly, of the single-point estimators the WAVG shows the least angular error and least total time, 14 min, above the threshold.

All of the single point estimators exhibit increased 3σ bounds for d_x and d_y and an increase in the mean angular error bias between 40 min and 50 min. This time corresponds to the region of the orbit where the spacecraft's sensors are most affected by Earth's albedo. Despite this, all three methods are able to maintain less than 15° angular error for 87 % of the time spent in view of the Sun.

Several biases are assumed small in the formulation of the estimation methods and the impact of that assumption can be seen in Fig. 6c, particularly for the WAVG and LSMN methods. The results show a significant bias in the estimate of d_z, the axis desired to be pointing directly at the Sun, due to the biases present in the system dynamics and measurement models. Despite the significant biases and noise, all methods are shown capable of achieving a power positive orientation using only CSS, a rate gyro, and reaction wheels. The EKF method is able to achieve approximately 4° accuracy at the 99th percentile.

Closed Loop Sun-Direction Estimation without Rate Gyro Measurements

The control used to reorient the spacecraft to a power positive state requires a measure of the spacecraft's angular velocity $\boldsymbol{\omega}$ in order to arrest any rotational rates. In addition, the EKF method requires the spacecraft's angular velocity for state propa-

gation. It is assumed the angular velocity of the spacecraft is nominally provided by a rate gyro, however, it may be necessary to turn off the rate gyro in a power critical situation or in a worst case scenario the rate gyro might fail. For this situation, the estimation approaches outlined previously are modified to use a simple estimate of the vehicle's angular velocity vector, a scaling of the cross product of the current and previous estimates of the sun-direction vector, given by

$$\bar{\boldsymbol{\omega}}_k = \frac{\hat{\boldsymbol{d}}_k \times \hat{\boldsymbol{d}}_{k-1}}{\left\| \hat{\boldsymbol{d}}_k \times \hat{\boldsymbol{d}}_{k-1} \right\|} \cos^{-1}\left(\frac{\hat{\boldsymbol{d}}_k^T \hat{\boldsymbol{d}}_{k-1}}{\left\| \hat{\boldsymbol{d}}_k \right\| \left\| \hat{\boldsymbol{d}}_{k-1} \right\|} \right) \frac{1}{t_k - t_{k-1}} \tag{28}$$

where $\hat{\boldsymbol{d}}_k$ is the best estimate of the scaled sun-direction unit vector at time t_k. This value is used in place of rate gyro measurements in the control to arrest vehicle rates.

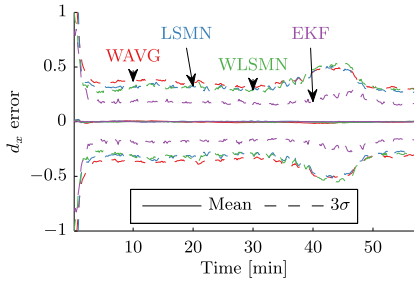

(a) Error in x-component of scaled sun-direction vector.

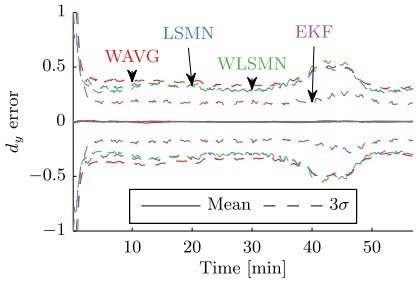

(b) Error in y-component of scaled sun-direction vector.

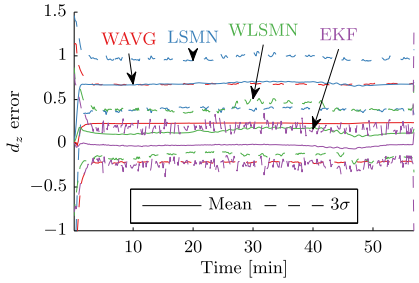

(c) Error in z-component of scaled sun-direction vector.

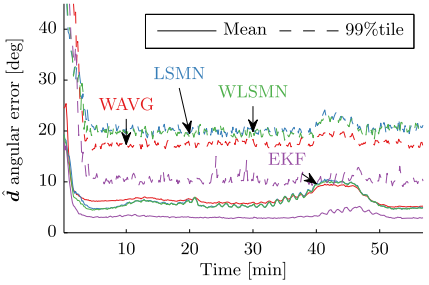

(d) Angular error of sun-direction vector estimate.

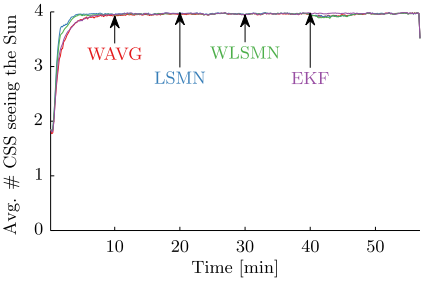

(e) Average number of CSS receiving direct sunlight.

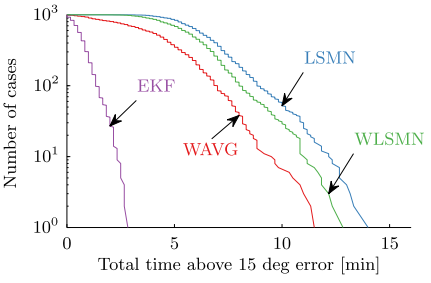

(f) Total time spent with estimate in error of greater than 15°.

Fig. 7 Calculated statistics for 1000 case Monte Carlo run with control, but no rate gyro measurements

To counteract the additional error introduced by numerical differencing, the estimate is conservatively bounded about each axis and run through a first order 10 Hz low-pass filter. Since the numerical simulation results shown later assume maximum initial angular rates of $2.0^\circ/s$ about each axis, the rates are conservatively constrained to $10^\circ/s$ about each axis before applying the low pass filter.

Results show that even though this simple backward-difference method does not provide new information, it does provide an adequate estimate for achieving a power positive orientation. More complicated methods for estimating the angular rate of a satellite exist; for example Azor, Bar-Itzhack, and Harman propose using an extended interlaced Kalman filter composed of three separate Kalman filters [34] and Mortari and Akela propose two filtering techniques that use quaternions to estimate the angular velocity [35]. Because the methods examined are shown to perform quite well using the simple method proposed here, the investigation of more complicated methods is left to future work.

Statistics are shown in Fig. 7 for a 1000 case Monte Carlo analysis where the control is operating, but no rate gyro measurements are available. It is important to remember this represents a worst case safe-mode scenario in which only CSS and reaction wheels are available, and is presented here as a preliminary look into the robustness of the estimation algorithms examined. Nominally, with rate gyro measurements, the sequential estimators propagate the spacecraft's orientation while in the shadow of the Earth. However, because the rate estimate is entirely dependent on having a sun-direction estimate, the sequential estimator propagation and all control effort are suspended when the spacecraft is in the shadow of the Earth if no rate gyro measurements are available.

As a result of the numerical differentiation, the single-point estimators perform approximately the same, albeit with much greater variability in the estimate, as when using an intermediate level gyro, as long as the low pass filtering mentioned is implemented. This is expected as the rate gyro measurement is only used by the control algorithm to damp out the spacecraft angular velocity. It is interesting that the EKF stills perform quite well despite the significant noise of the rate measurements. All EKF cases spend less than approximately 5 min of the 56 min in view of the Sun per orbit with estimation error greater than 15°.

Conclusions

Several methods for estimating and controlling a spacecraft's orientation relative to the Sun using only coarse sun sensor and rate gyro measurements are reviewed and compared. Of interest is how to achieve a power positive orientation when little information is available, such as immediately post launch vehicle separation or in a power critical safe-mode situation. All methods perform simultaneous sun-direction estimation and attitude control to achieve a power-positive orientation. The first method uses a simple vector average calculation, the second and third involve variations on a combination of least squares and minimum norm criteria, and the final incorporates an extended Kalman filter.

Nominally, with rate gyro measurements available, the EKF method provides the most accurate estimate despite significant dynamic and measurement biases, reducing the 3σ pointing error of the sun-direction estimate below 4°. The single point estimators investigated benefit significantly from the application of simultaneous control effort decreasing their error by half. It is shown that all approaches are capable of estimating a scaled sun-direction vector without rate gyro measurements, using only a simple backward difference method to estimate angular rates, thus providing promising performance for safe-mode operation in a situation with little observability.

References

1. Puig-Suari, J., Turner, C., Twiggs, R.J.: CubeSate: The Development and Launch Support Infrastructure for Eighteen Different Satellite Customers on One Launch, Proceedings of the AIAA/USU Conference on Small Satellites, Logan, UT, ISBN 6507238651, pp. 1–5 (2001)
2. Bouwmeester, J., Guo, J.: Survey of worldwide pico- and nanosatellite missions, distributions and subsystem technology. Acta Astronaut. **67**(7-8), 854–862 (2010). doi:10.1016/j.actaastro.2010.06.004. ISSN 00945765
3. Rufino, G., Grassi, M., Rolfi, M.: Preliminary Calibration Results For a High-Precision CMOS Sun Sensor, Proceedings of the AIAA Guidance, Navigation, and Control Conference and Exhibit, Honolulu, HI, 1–9 (2011)
4. Ninomiya, K., Ogawara, Y., Tsuno, K., Akabane, S.: High Accuracy Sun Sensor Using CCDs, Proceedings of the AIAA Guidance, Navigation, and Control Conference, American Institute of Aeronautics and Astronautics, Minneapolis, MN (1988)
5. Black, H.D.: A Passive System for Determing the Attitude of a Satellite. AIAA J. **2**(7), 1350–1351 (1964)
6. Davenport, P.B.: A Vector Approach to the Algebra of Rotations with Applications, Tech. Rep. August, National Aeronautics and Space Adminstration, Goddard Space Flight Center, Greenbelt, MD (1968)
7. Shuster, M.D., Oh, S.D.: Three-Axis Attitude Determination from Vector Observations. J. Guid. Control. Dyn. **4**(1), 70–77 (1981). doi:10.2514/3.19717. ISSN 0731-5090
8. Markley, F.L.: Attitude Determination Using Vector Observations: A Fast Optimal Matrix Algorithm. J. Astronaut. Sci. **41**(2), 261–280 (1993)
9. Mortari, D., Markley, F.L., Singla, P.: Optimal Linear Attitude Estimator. J. Guid. Control. Dyn. **30**(6), 1619–1627 (2007). doi:10.2514/1.29568. ISSN 0731-5090
10. Appel, P.: Magnetometer, Attitude Estimation from Measurements, Earth-Albedo-Corrected Coarse Sun Sensor. Acta Astronaut. **56**(1-2), 2–5 (2005). doi:10.1016/j.actaastro.2004.09.001. ISSN 00945765
11. Jung, H., Psiaki, M.L.: Tests of Magnetometer/Sun-Sensor Orbit Determination Using Flight Data, Proceedings of the AIAA Guidance, Navigation, and Control Conference and Exhibit, American Institute of Aeronautics and Astronautics, Montreal, Canada (2001)
12. Jackson, B., Carpenter, B.: Optimal Placement of Spacecraft Sun Sensors Using Stochastic Optimization, Proceedings of the IEEE Aerospace Conference, IEEE, Big Sky, MT, ISBN 0780381556104, 3916–3923 (2004)
13. Springmann, J.C., Cutler, J.W.: Optimization of Directional Sensor Orientation with Application to Photodiodes for Spacecraft Attitude Determination, Proceedings of the AAS/AIAA Space Flight Mechanics Conference, Kauau, HI,1–19 (2013)
14. Lerner, G.M.: Spacecraft Attitude Determination and Control, pp. 155–166. D. Reidel Publishing Co., Dordrecht, The Netherlands (1978)
15. Krivova, N.a., Vieira, L.E.a., Solanki, S.K.: Reconstruction of solar spectral irradiance since the Maunder minimum. J. Geophys. Res. **115**(A12) (2010). doi:10.1029/2010JA015431. ISSN 0148-0227

16. Flatley, T.W., Moore, W.A.: An Earth Albedo Model: A Mathematical Model for the Radiant Energy Input to an Orbiting Spacecraft Due to the Diffuse Reflectance of Solar Radiation From the Earth Below, Tech. rep., National Aeronautics and Space Administration, Goddard Space Flight Center, Greenbelt, MD (1994)
17. Bhanderi, D.D.V., Bak, T.: Modeling Earth Albedo for Satellites in Earth Orbit, Proceedings of the AIAA Guidance, Navigation, and Control Conference and Exhibit, American Institute of Aeronautics and Astronautics, San Francisco, CA (2005)
18. Snyder, J.P.: Map Projections: A Working Manual. Geol. Surv. (U.S.) Prof. Pap. **1395**, 76–85 (1987)
19. Knuth, D.: Two Notes on Notation. Am. Math. Mon. **99**(5), 403–422 (1992)
20. Tapley, B., Schutz, B., aBorn, G.: Statistical Orbit Determination, Elsevier Academic Press, ISBN 9780126836301 (2004)
21. Crassidis, J.L., Junkins, J.L.: Optimal Estimation of Dynamic Systems. Boca Raton, FL (2004)
22. Simon, D.: Optimal State Estimation, John Wiley & Sons, Inc. (2006)
23. Schaub, H., Junkins, J.L.: Analytical Mechanics of Space Systems, chap. 3, AIAA Education Series, Reston, VA, 2nd ed., pp. 79–142 (2009)
24. Springmann, J.C.: On-Orbit Calibration of Photodiodes for Attitude Determination, Proceedings of the AIAA/USU Conference on Small Satellites, Logan, UT (2013)
25. Farrenkopf, R.L.: Analytic Steady-State Accuracy Solutions for Two Common Spacecraft Attitude Estimators. J. Guid. Control. Dyn. **1**(4), 282–284 (1978). doi:10.2514/3.55779. ISSN 0731-5090
26. Van Trees, H.L.: Detection, Estimation and Modulation Theory, Part I, John Wiley & Sons, Inc. (1968)
27. Tichavský, P., Muravchik, C.H., Nehorai, A.: Posterior Cramér-Rao Bounds for Discrete-Time Nonlinear Filtering. IEEE Trans. Signal Process. **46**(5), 1386–1396 (1998). doi:10.1109/78.668800. ISSN 1053-587X
28. Leven, W.F.: Approximate Cramér-Rao Bounds for Multiple Target Tracking, Doctor of philosophy, Georgia Institute of Technology (2006)
29. Woodbury, D.P., Junkins, J.L.: On the Consider Kalman Filter, AIAA Guidance, Navigation, and Control Conference, American Institute of Aeronautics and Astronautics, Toronto, ON, doi:10.2514/6.2010-7752 (2010)
30. Zanetti, R., Bishop, R.H.: Kalman Filters with Uncompensated Biases. J. Guid. Control. Dyn. **35**(1), 327–335 (2012). doi:10.2514/1.55120. ISSN 0731-5090
31. Acton, C.: Ancillary Data Services of NASA's Navigation and Ancillary Information Facility. Planet. Space Sci. **44**(1), 65–70 (1996)
32. Hogan, E.A., Schaub, H.: Three-Axis Attitude Control using Redundant Reaction Wheels with Continuous Momentum Dumping, Proceedings of the AAS/AIAA Spaceflight Mechanics Conference, American Institute of Aeronautics and Astronautics, Kauai, HI (2013)
33. Horn, R.A., Johnson, C.R.: Topics in Matrix Analysis, chap. 5, Cambridge University Press, 298–381 (1991)
34. Azor, R., Bar-Itzhack, I.Y., Harman, R.R.: Satellite Angular Rate Estimation from Vector Measurements. J. Guid. Control. Dyn. **21**(3) (1998). doi:10.2514/2.4257. ISSN 0731-5090
35. Mortari, D., Akella, M.R.: Discrete and Continuous Time Adaptive Angular Velocity Estimators, Proceedings of the AAS/AIAA Space Flight Mechanics Conference, Williamsburg, VA (2015)